Impact of Noise Power Uncertainty on the Performance of Wideband Spectrum Segmentation

Selçuk TAŞCIOĞLU [1], Oktay ÜRETEN [2], Ziya TELATAR [1]

[1] Electronics Engineering Department, Ankara University, 06100 Ankara, Turkey
[2] Communications Research Centre, Terrestrial Wireless Systems Research Branch, Ottawa, ON, Canada K2H 8S2

{selcuk.tascioglu, ziya.telatar}@eng.ankara.edu.tr, oktay.ureten@crc.gc.ca

Abstract. *The objective of this work is to investigate the impact of noise uncertainty on the performance of a wideband spectrum segmentation technique. We define metrics to quantify the degradation due to noise uncertainty and evaluate the performance using simulations. Our simulation results show that the noise uncertainty has detrimental effects especially for low SNR users.*

Keywords

Cognitive radio, spectrum sensing, wideband RF spectrum monitoring, noise uncertainty, Markov chain Monte Carlo.

1. Introduction

The typical operating environment of a cognitive radio (CR) will furnish heterogeneous networks with diverse characteristics. Network nodes will adapt to the operating environment by modifying transmission characteristics; therefore, parameters such as signal and interference levels, channel allocations and operating frequencies will be changing constantly. The requirement for detecting signals in such environments poses several challenges. Locating an unused spectrum within a large bandwidth will be time consuming without having prior knowledge about the operating frequencies and bandwidths and setting a proper detection threshold level will become cumbersome.

Increasing number of papers focus on addressing the challenges of wideband sensing. In [1], a dual-stage approach combines coarse and fine sensing schemes for more efficient wideband sensing. In [2], a bank of multiple narrowband detectors is jointly optimized to improve opportunistic throughput capacity of cognitive radios. In [3]-[5], the wideband spectrum identification task is formulated as a spectral edge detection problem and the discontinuities in the power spectrum density are identified using wavelet [3], phase-field segmentation [4] and reversible jump Markov chain Monte Carlo (RJMCMC) [5] techniques.

One of the important issues in spectrum sensing is the impact of uncertainty in noise power measurements. Channel noise cannot be measured perfectly due to measurement uncertainties. The uncertainties in the noise power knowledge put fundamental limits on the detection performance. In [6], it is shown that the detection of spread spectrum signals by a wideband energy detector becomes more difficult as the SNR required for detection becomes a function of noise uncertainty only and is independent of the observation interval. This effect is called "SNR wall" in [7] and an extensive analysis of the impact of noise uncertainty is provided by considering general classes of signals and detection algorithms. The impact of noise uncertainty has also been verified experimentally using controlled experiments in [8].

Recently, noise uncertainty issues have been addressed within the scope of wideband sensing. In [9], spectrum sensing of several subbands when the background noise has an unknown variance is considered and an invariant generalized likelihood ratio detector is proposed. In [10], maximum likelihood estimation of the noise and signal power levels from samples of a wideband signal comprising multiple multicarrier channels is considered and a recursive estimation method is proposed. As a remedy to overcome noise uncertainty, the use of multiple antennas has been explored in [11] and [12].

The segmented periodogram approach proposed for wideband spectrum sensing developed in [5] requires noise power to be known exactly at the receiver. It is anticipated that the noise uncertainty will affect the performance of the segmentation technique and the objective of this study is to investigate its impact and to quantify the degradation using simulations.

The presentation of the paper is as follows: In Section 2, the segmented periodogram concept is presented. In Section 3 performance metrics introduced. Simulation setup and performance simulation results under noise uncertainty are presented in Section 4. Finally, Section 5 concludes the paper.

2. Segmented Periodogram

The periodogram and its improvements are common tools for spectrum estimation mostly because computationally efficient FFT algorithms can be used in the calculations. Even though the periodogram is an inconsistent estimate of the power spectrum, periodogram ordinates are a set of sufficient statistics for the corresponding spectral density function's parameters [13]. Therefore a suitable smoothed version of the raw periodogram can produce good estimates of the power spectral density.

There are several ways to improve the raw periodogram estimate: averaging a number of different periodograms (Bartlett procedure), applying a window to the estimated sample correlation function before transforming (Blackman and Tukey) or combining windowing and averaging (Welch periodogram). All of these improved methods reduce the variance of the estimated spectrum in exchange for increasing its bias. Alternatively, data samples weighted using a number of orthogonal window functions (tapers) can be averaged to reduce the variance of spectral estimates (multi-taper method-MTM). The MTM method provides a time-bandwidth parameter which is used to balance the variance and resolution.

In the segmented periodogram approach [5], a multiple change point analysis of the raw periodogram of the RF spectrum is developed, in which the spectra are separated into noise and signal segments by an unknown number of change-points, with each signal segment assumed to have been generated by a transmission. The number of users, their transmission frequencies and bandwidths are treated as random variables, and the posterior distributions of these parameters are obtained by updating prior distributions using the observed data. The marginal distributions of the parameters cannot be obtained analytically for this problem; therefore a numerical solution based on generating simulated samples from the posterior distributions of the parameters is utilized. These samples are then used to obtain a smoothed power spectrum estimate from which the number of users, their spectral edges and received power levels can be obtained. As the smoothing is performed by averaging over random realizations of the underlying power spectrum inferred using the simulated samples, neither increasing the data length nor reducing the resolution is required.

A piece-wise flat RF spectrum assumption can be justified based on the characteristics of practical radio communication signals. In such systems, the power spectra of transmitted signals are strictly shaped to fit into sharp transmission masks to avoid interference into the neighboring channels. The use of filters with sharp transition bands is also important for better utilization of the spectrum as this allows for stacking more channels into a given spectrum segment. From the radio spectrum monitoring and dynamic spectrum allocation perspective, the goal is to locate used/unused parts of the spectrum, rather than to extract the detailed spectral shape of the transmissions. For these purposes, it is not unrealistic to assume that the observed wide band RF spectrum data can be modeled as a piece-wise flat multiple change-point process. The piece-wise flat RF spectrum concept has also been utilized in [3], [4] in the context of wide-band spectrum sensing.

2.1 Mathematical Model

Assuming the noise samples at the receiver are independent and Gaussian distributed, the periodogram ordinates, excluding the DC component, will be independent and chi-square distributed with two degrees of freedom

$$Y(k) \sim \chi_2^2(\sigma^2, \lambda(k)) \tag{1}$$

where k is frequency bin number, $\sigma^2 = \sigma_n^2 N/2$, σ_n^2 and N are the noise power and the DFT size, respectively. The noncentrality parameter is given by the function $\lambda(k)$ corresponding to the received signal power for the kth bin in the absence of noise. The probability density function (pdf) of the χ_2^2 distribution is given by

$$p(x) = \frac{1}{2\sigma^2} I_0\left(\sqrt{\frac{\lambda x}{\sigma^2}}\right) e^{\left(-\frac{\lambda+x}{2\sigma^2}\right)}, \quad x > 0 \tag{2}$$

where $I_0(x)$ is the zero order modified Bessel function of the first kind. Note that the noncentrality parameter $\lambda(k) = 0$ for noise only bins, and $\lambda(k) \neq 0$ for signal bins.

We assume that the noncentrality function $\lambda(.)$ is a step function and there are m change points at positions s_j. The noncentrality function then forms a piecewise flat function for $k = 1,\ldots,N$

$$\lambda(k) = h_j, \quad s_j < k \leq s_{j+1}, \quad j = 0, \ldots, m \tag{3}$$

where h_j is the height of jth segment located between the sample points s_j+1 and s_{j+1}. Note that $s_0 = 0$ and $s_{m+1} = N$ by definition.

Suppose there is a countable collection of candidate models $\mathtt{M}_m$, $m \in \{0, 1, \ldots, M_p\}$, where M_p is the maximum number of change points. Our assumption is that there are at most $M_p/2$ transmissions within the observed spectrum. Model $\mathtt{M}_m$ has a vector of unknown parameters θ^m which consists of $s = [s_1\, s_2 \ldots s_m]$ and $h = [h_0\, h_2 \ldots h_m]$, assumed to lie in Θ^m. The general parameter space Θ can be written as the union of each subspace

$$\Theta = \bigcup_{m=0}^{M_p} \{m\} \times \Theta^m \tag{4}$$

where each subspace Θ^m contains change locations and their heights for the model order m. Given a noisy power spectrum data $Y(k)$, the objective is to estimate m and θ^m, i.e. the number of users, their spectral band edges and power levels. Fig. 1 shows a representation of a typical radio spectrum together with the parameters to be estimated.

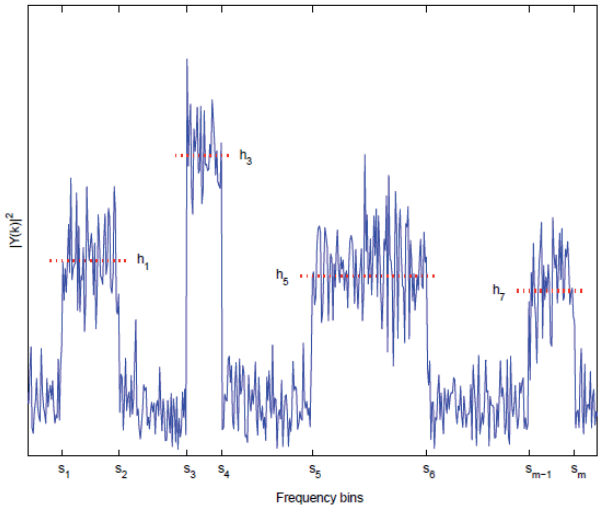

Fig. 1. A representation of a typical radio spectrum.

A numerical solution to this parameter estimation problem is given in [5]. The approach presented in [5] is based on obtaining simulated samples from the posterior distribution of the model parameters using reversible jump Markov chain Monte Carlo (RJMCMC) technique [14]. These samples are then used to reconstruct the estimated posterior mean $E\{\lambda(k)|Y\}$ by averaging $T_{\hat{m}}$ piece-wise flat functions, f, created using $\theta^{\hat{m}}$ for $\hat{m}$

$$\hat{\lambda} = \frac{1}{T_{\hat{m}}} \sum_{t=1}^{T_{\hat{m}}} f_k^{(\hat{m})}(\theta_t^{\hat{m}}) \tag{5}$$

where $T_{\hat{m}}$ is the number of samples drawn from the posterior and $\hat{m}$ is called the marginal maximum a posteriori (MMAP) estimate of m given below

$$\hat{m} = \underset{m \in \{0,1,\ldots,M_p\}}{\arg\max}\ p(m \mid Y) \tag{6}$$

The details of the algorithm can be found in [5].

3. Performance Metrics

Three sets of performance metrics are defined to assess the performance degradation due to noise uncertainty. The first group of metrics is based on the mean squared distance between the actual and the estimated spectrum, which can be regarded as reconstruction error.

Let λ denote the actual discrete power spectra and $\hat{\lambda}$ be an estimate of λ obtained using the RJMCMC algorithm explained in Section 2. The total mean squared error of the reconstruction is calculated as

$$MSE = \frac{1}{N-1} \sum_{k=1}^{N-1} (\lambda[k] - \hat{\lambda}[k])^2 \tag{7}$$

where k is the frequency bin index and N-1 is the total number of periodogram bins excluding DC component.

In order to distinguish between errors in noise and signal bins, partial mean squared errors can be defined for noise and signal segments only

$$MSE_{signal} = \frac{1}{N_{signal}} \sum_{k \in \psi} (\lambda_\psi[k] - \hat{\lambda}_\psi[k])^2, \tag{8}$$

$$MSE_{noise} = \frac{1}{N_{noise}} \sum_{k \in \nu} (\lambda_\nu[k] - \hat{\lambda}_\nu[k])^2 \tag{9}$$

where ψ and $\boldsymbol{\nu}$ are the sets of periodogram bins containing signal and noise components, and N_{signal} and N_{noise} are the numbers of signal and noise only bins, respectively. MSE_{signal} and MSE_{noise} measure the reconstruction errors in signal and noise bins, and MSE is the total reconstruction error. Note that $MSE \neq MSE_{signal} + MSE_{noise}$.

The second set of metrics is defined based on the numbers of erroneous detection decisions, namely missed detections and false alarms. These metrics measure the effect of noise uncertainty on the detection performance when a segmented periodogram is employed in sensing. A missed detection error occurs when a signal bin is declared to be a noise bin whereas a false alarm occurs when a noise bin is declared as a signal bin. The ratios of missed detection, false alarm and total error rate are defined by

$$P_M = \frac{N_{miss}}{N_{signal}}, \tag{10}$$

$$P_F = \frac{N_{false}}{N_{noise}}, \tag{11}$$

$$P_E = \frac{N_{error}}{N-1} \tag{12}$$

where N_{miss}, N_{false} and N_{error} are the total numbers of missed detections, false alarms and total errors, respectively. Note that the number of total detection errors N_{error} is the sum of false alarms and missed detections.

The last metric proposed to evaluate the performance is the model order estimation error, which is defined as

$$M_e = \hat{m} - m \tag{13}$$

where m and $\hat{m}$ are the actual and estimated numbers of spectral edges. Note that the number of spectral edges determines the number of segments and therefore relates to the number of active users within the observation bandwidth.

4. Performance Evaluation

The performance evaluation of the segmentation algorithm under noise uncertainty is accomplished using randomly generated periodograms. Each randomly generated

periodogram has 1024 bins and contains a number of active users with varying bandwidths, carrier frequencies and power levels. In all performance evaluation simulations in this paper, the number of users and the bandwidth of each user are drawn from the discrete uniform distributions $U\{1, \ldots, 10\}$ and $W_i \sim U\{30,\ldots,60\}$, respectively and the users are placed at randomly selected locations.

In the simulations, the proposed metrics are calculated for a given user *SNR*, which is defined as

$$SNR = 10\log_{10}\frac{\lambda}{2\sigma^2} \tag{14}$$

where λ is the received power of the user and σ^2 is the variance of both real and imaginary components of the noise.

Monte Carlo simulations are used for performance evaluations. In each simulation, the RJMCMC algorithm is run on a randomly generated periodogram. The RJMCMC algorithm is initialized with the following priors: Gamma distribution $h \sim \Gamma(\alpha,\beta)$ with $\alpha = 1$ and $\beta = 0.02$ is used for segment heights. The number of change points is drawn from Poisson distribution $m \sim Pois(\Lambda)$ with $\Lambda = 1$ and a maximum support restriction of 40. For the change point locations even-numbered order statistics is employed [14].

The RJMCMC algorithm simulates 10000 samples and the MMAP model order is estimated from 7000 samples after 3000 burn-in samples. The simulated samples that are from the MMAP model order are then used to reconstruct a segmented periodogram by calculating the posterior expectations as explained in Section 2. The errors are calculated for 1000 random periodograms and averaged over the simulations for each user SNR of 2 to 20 dB at 1 dB intervals. In the evaluation of noise power uncertainty, mismatch values of -3 to +3 dB at 0.5 dB intervals are added to the actual noise power. The RJMCMC algorithm is initiated with the assumed noise power as the actual noise power is not available.

4.1 Reconstruction Performance

The average mean squared reconstruction error versus user SNR is plotted in Fig. 2 (solid), showing that reconstruction error decreases as the user SNR increases. This is because the segmentation algorithm is able to estimate spectral heights more accurately as high-SNR users create spectral edges that are easier to locate.

Fig. 2 also shows the performance under uncertainty (dashed). The reconstruction error is higher when there is uncertainty in noise power. Note that the impact of noise uncertainty is more significant when the user SNRs are lower. At high SNRs, reconstruction performance degradation due to noise uncertainty is negligible.

The mean squared reconstruction error versus noise power uncertainty is shown in Fig. 3 (solid). As seen from Fig. 3, the reconstruction error is minimum when noise uncertainty is zero and the performance degrades as the amount of uncertainty increases for both over and underestimation cases. Note that the performance degradation due to overestimation is more significant than that for underestimation.

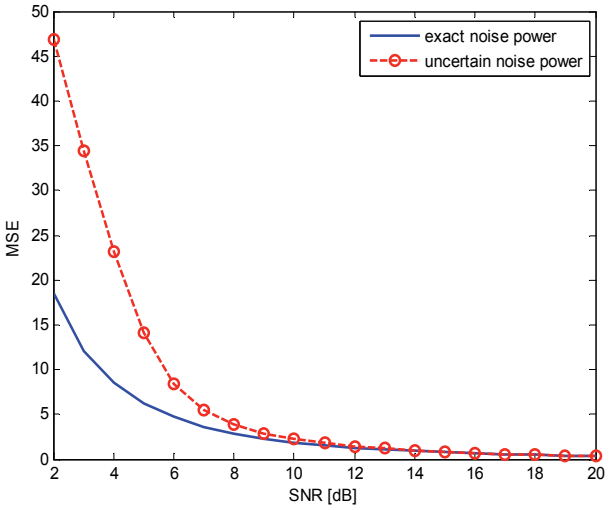

Fig. 2. MSE versus user SNR.

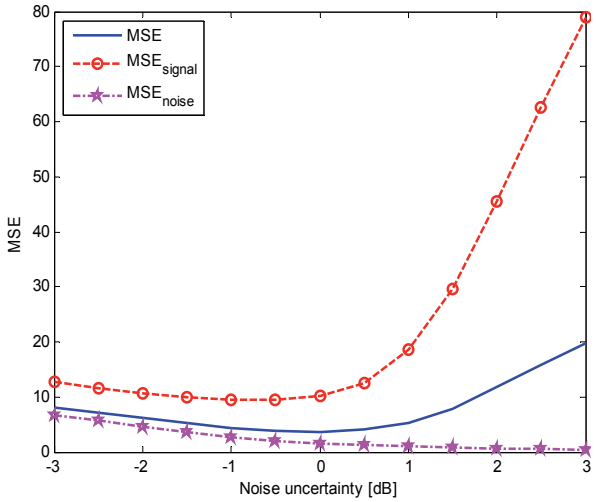

Fig. 3. MSE versus noise power uncertainty.

Also plotted in Fig. 3 are reconstruction error curves for signal and noise bins separately. It is observed from these curves that overestimation of the noise power results in improved noise level estimates; however the performance degradation due to signal level estimates dominates the total error producing a net performance loss. This is because signal levels are higher than the noise levels for the tested user SNRs and therefore contribute more to the error sum. Note that the errors in the signal level estimates are negligible when the noise power is underestimated.

4.2 Detection Performance

The number of missed detections and false alarms were calculated for randomly generated periodograms by

comparing the value of each segmented periodogram bin to a threshold value, which was set to be the noise floor of $2\sigma^2$. The total detection error rate averaged over 1000 simulations for each user SNR of 2 to 20 dB at 1 dB intervals are plotted in Fig. 4 (solid).

Also shown in Fig. 4 are the detection errors under noise uncertainty (dashed curves). As seen from this figure, there is about 10% loss in total detection rate between uncertain and perfect noise power cases in lower user SNRs. As the user SNR increases, the performance loss due to noise power uncertainty becomes negligible.

Fig. 5 shows the missed detections and false alarms versus noise power uncertainty. This figure shows that overestimating the noise power has a negligible effect on the false alarm rate; however the missed detection rate deteriorates significantly as the amount of overestimation increases. Underestimating the noise power mostly affects the false alarm rate. Even though the increase in false alarm rate is less than 5% for underestimation levels of less than 2 dB, the performance deteriorates significantly when the underestimation amount exceeds 2 dB.

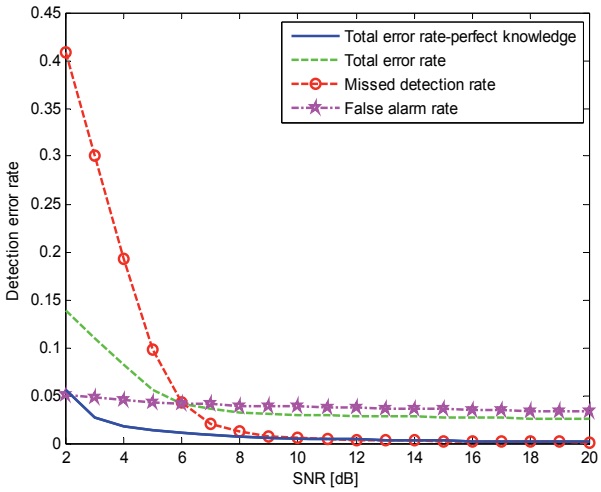

Fig. 4. Missed detection and false alarm ratios versus SNR.

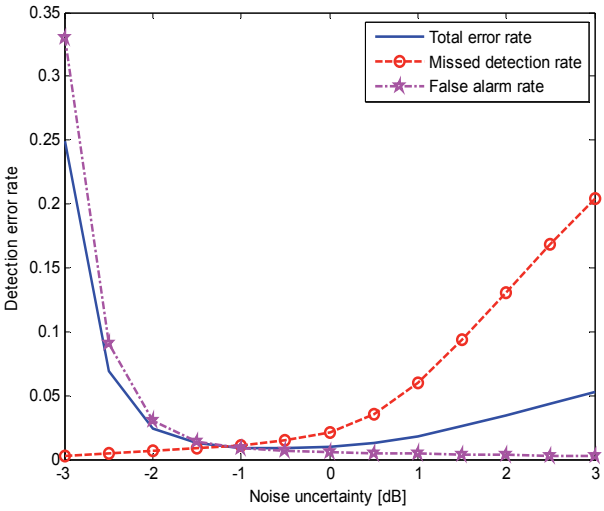

Fig. 5. Missed detection and false alarm ratios versus noise power uncertainty.

4.3 Model Order Estimation Errors

The cumulative mass functions of the model estimation errors are shown in Fig. 6. As seen from this figure, underestimating the noise power results in overestimation of the number of users (false users are detected). If the noise power is overestimated then the number of users is underestimated (missed users).

Model order estimation errors at various noise uncertainty levels are shown in Fig. 7 as a function of the user SNR. As seen from the figure, model order estimation error decreases as the SNR increases, even for higher noise uncertainty values.

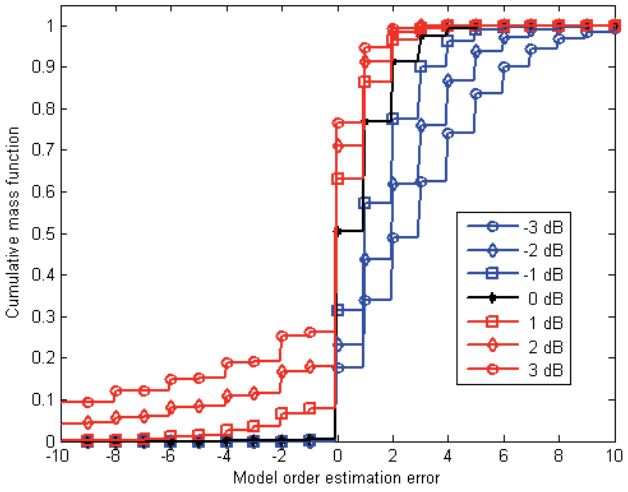

Fig. 6. Cumulative mass function of the model order estimation error.

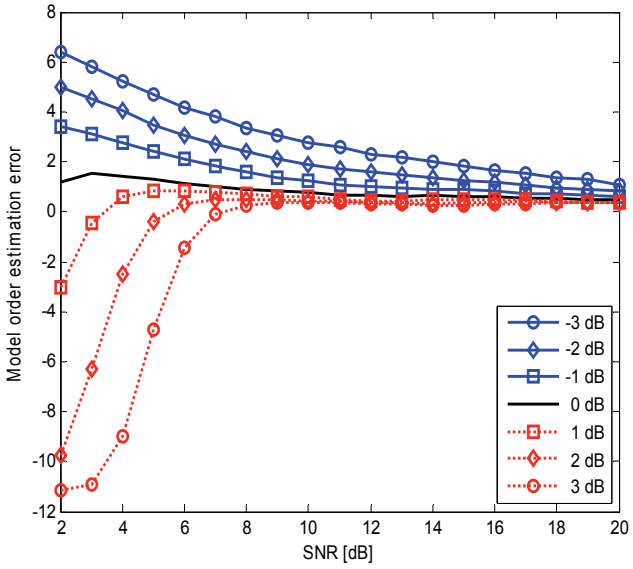

Fig. 7. Model order estimation error versus SNR.

5. Conclusions

In this work, the impact of the noise uncertainty on the detection and reconstruction performance of the seg-

mented periodogram technique is investigated. Simulation results show that noise power uncertainty degrades both detection and reconstruction performances.

The impact of noise uncertainty is more detrimental for low SNR users. However, detection degradation performance in low SNRs is negligible when the noise uncertainty is low.

The over and underestimation of the noise power affects the estimation accuracy in signal and noise segments, respectively. Similarly, noise power overestimation results in increased missed users whereas noise power underestimation generates false users.

In order to alleviate noise power uncertainty issues noise power can be treated as a nuisance parameter and estimated together with the rest of the parameters in the RJMCMC algorithm. This will be addressed in future work.

References

[1] HUR, Y., PARK, J., WOO, W., LIM, K., LEE, C.-H., KIM, H. S., LASKAR, J. A wideband analog multi-resolution spectrum sensing (MRSS) technique for cognitive radio (CR) systems. In *IEEE Int. Symp. on Circuits and Syst.*, May 2006, p. 4090–4093.

[2] QUAN, Z., CUI, S., SAYED, A. H., POOR, H. V. Wideband spectrum sensing in cognitive radio networks. In *IEEE Int. Conf. on Commun.*, May 2008, p. 901–906.

[3] TIAN, Z., GIANNAKIS, G. B. A wavelet approach to wideband spectrum sensing for cognitive radios. In *1st Int. Conf. on Cognitive Radio Oriented Wireless Networks and Commun.*, June 2006, p. 1–5.

[4] ESLAMI, M., SADOUGH, S. M.-S. Wideband spectrum sensing for cognitive radio via phase-field segmentation. In *6th Conference on Wireless Advanced (WiAD),* 27-29 June 2010, p.1-5.

[5] TASCIOGLU, S., URETEN, O. Bayesian wideband spectrum segmentation for cognitive radios. In *Proceedings of 18th International Conference on Computer Communications and Networks, ICCCN 2009*, 3-6 Aug. 2009, p.1-6.

[6] SONNENSCHEIN, A., FISHMAN, P. M. Radiometric detection of spread-spectrum signals in noise of uncertain power. *IEEE Transactions on Aerospace and Electronic Systems*, 1992, vol. 28, no. 3, p. 654–660.

[7] TANDRA, R., SAHAI, A. SNR walls for signal detection. *IEEE J. Sel. Topics Signal Process.,* Feb. 2008, vol. 2, no. 1, p. 4–17.

[8] CABRIC, D., TKACHENKO, A., BRODERSEN, R. W. Spectrum sensing measurements of pilot, energy, and collaborative detection. In *Military Communications Conference, MILCOM 2006*. Washington (DC, USA), 2006, p. 1–7.

[9] TAHERPOUR, A., NASIRI-KENARI, M., GAZOR, S. Invariant wideband spectrum sensing under unknown variances. *IEEE Transactions on Wireless Communications,* May 2009, vol.8, no. 5, p.2182-2186.

[10] LOPEZ-VALCARCE, R., VAZQUEZ-VILAR, G. Wideband spectrum sensing in cognitive radio: Joint estimation of noise variance and multiple signal levels. In *IEEE 10th Workshop on Signal Processing Advances in Wireless Communications, SPAWC '09,* 21-24 June 2009, p.96-100.

[11] TAHERPOUR, A., NASIRI-KENARI, M., GAZOR, S. Multiple antenna spectrum sensing in cognitive radios. *IEEE Transactions on Wireless Communications,* 2010, vol. 9, no. 2, p. 814-823.

[12] LOPEZ-VALCARCE, R., VAZQUEZ-VILAR, G., SALA, J. Multiantenna spectrum sensing for cognitive radio: overcoming noise uncertainty. In *The 2nd International Workshop on Cognitive Information Processing CIP 2010,* June 2010, p. 310-315.

[13] PRIESTLEY, M. B. Spectral analysis and time series. *Academic Press Limited,* London, 1994.

[14] GREEN, P. J. Reversible jump Markov chain Monte Carlo computation and Bayesian model determination. *Biometrika,* 1995, vol. 82, no. 4, p. 711–732.

About Authors ...

Selçuk TAŞCIOĞLU received his B.Sc. and M.Sc. degrees from Ankara University in 2001 and 2004, respectively. He is currently a Ph.D. student in Electronics Engineering Department, Ankara University. His current research interest is spectrum sensing in cognitive radio networks.

Oktay ÜRETEN received his Ph.D. in Electronics Engineering at the University of Ankara, Turkey in 2000. Dr. Üreten is a research scientist at the Communications Research Centre in Ottawa, where he has been working since 2001. His current research is focused on dynamic spectrum access networks.

Ziya TELATAR received his B.Sc. degree in Electronics and Telecommunications Engineering from Yildiz Technical University, Turkey, in 1983 and M.Sc. and Ph.D. degrees in Electronics Engineering from Ankara University in 1993 and 1996, respectively. Dr. Telatar joined the Department of Electronics Engineering at Ankara University in 1990, where he is currently working as Associate Professor. His research interests include image restoration, recognition, motion estimation, biomedical signal and image processing.